Equilibrium and traveling-wave solutions of plane Couette flow

By J. HALCROW, J. F. GIBSON AND P. CVITANOVIĆ

School of Physics, Georgia Institute of Technology, Atlanta, GA 30332, USA

(Printed 25 October 2008)

We survey equilibria and traveling waves of plane Couette flow in small periodic cells at moderate Reynolds number Re, adding in the process eight new equilibrium and two new traveling-wave solutions to the four solutions previously known. Bifurcations under changes of Re and spanwise period are examined. These non-trivial flow-invariant unstable solutions can only be computed numerically, but they are 'exact' in the sense that they converge to solutions of the Navier-Stokes equations as the numerical resolution increases. We find two complementary visualizations particularly insightful. Suitably chosen sections of their $3D$-physical space velocity fields are helpful in developing physical intuition about coherent structures observed in moderate Re turbulence. Projections of these solutions and their unstable manifolds from ∞-dimensional state space onto suitably chosen 2- or 3-dimensional subspaces reveal their interrelations and the role they play in organizing turbulence in wall-bounded shear flows.

1. Introduction

In Gibson *et al.* (2008*b*) (henceforth referred to as GHC) we have utilized exact equilibrium solutions of the Navier-Stokes equations for plane Couette flow in order to illustrate a visualization of moderate Re turbulent flows in an infinite-dimensional state space, in terms of dynamically invariant, intrinsic, and representation independent coordinate frames. The state space portraiture (figure 1) offers a visualization of numerical (or experimental) data of transitional turbulence in boundary shear flows, complementary to $3D$ visualizations of such flows (figure 2). Side-by-side animations of the two visualizations illustrate their complementary strengths (see Gibson (2008*b*) online simulations). In these animations, $3D$ spatial visualization of instantaneous velocity fields helps elucidate the physical processes underlying the formation of unstable coherent structures, such as the Self-Sustained Process (SSP) theory of Waleffe (1990, 1995, 1997). Running concurrently, the ∞-dimensional state space representation enables us to track unstable manifolds of equilibria of the flow, the heteroclinic connections between them (Halcrow *et al.* 2008), and gain new insights into the nonlinear state space geometry and dynamics of moderate Re wall-bounded shear flows such as plane Couette flow.

Here we continue our investigation of exact equilibrium and traveling-wave solutions of Navier-Stokes equations, this time tracking them adiabatically as functions of Re and periodic cell size $[L_x, 2, L_z]$ and, in the process, uncovering new invariant solutions, and determining new relationships between them.

The history of experimental and theoretical advances is reviewed in GHC, Sect. 2; here we cite only the work on equilibria and traveling waves directly related to this investigation. Nagata (1990) found the first pair of nontrivial equilibria, as well as the first traveling wave in plane Couette flow (Nagata 1997). Waleffe (1998, 2003) computed

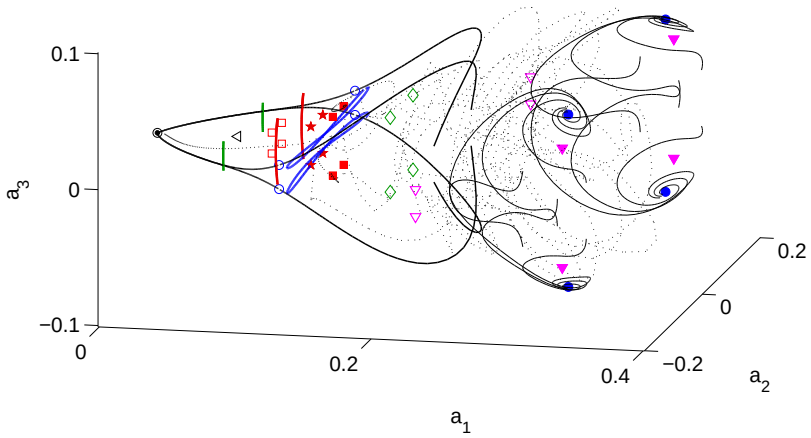

FIGURE 1. A 3-dimensional projection of the ∞-dimensional state space of plane Couette flow in the periodic cell $\Omega_{\rm W03}$ at $Re = 400$, showing all equilibria and traveling waves discussed in § 4. Equilibria are marked: ⊙ EQ_0, ○ EQ_1, ● EQ_2, □ EQ_3, ■ EQ_4, ◊ EQ_5, ◁ EQ_7, ★ EQ_9, ▽ EQ_{10}, ▼ EQ_{11}. Traveling waves trace out closed orbits: the spanwise-traveling TW_1 (blue loops), streamwise TW_2 (green lines), and TW_3 (red lines). In this projection the latter two streamwise traveling waves appear as line segments. The $\mathrm{EQ}_1 \to \mathrm{EQ}_0$ heteroclinic connections and the S-invariant portion of EQ_1 and EQ_2 unstable manifolds are shown with black lines. The cloud of dots are temporally equispaced points on a long transiently turbulent trajectory, indicating the natural measure. The projection is onto the translational basis (3.13) constructed from equilibrium EQ_2.

Nagata and other equilibria guided by the SSP theory. Other traveling waves were computed by Viswanath (2008) and Jiménez *et al.* (2005). Schmiegel (1999) computed and investigated a large number of equilibria. His 1999 Ph.D. provides a wealth of ideas and information on solutions to plane Couette flow, and in many regards the published literature is still catching up this work. GHC added the dynamically important 'newbie' $\mathbf{u}_{\rm NB}$ equilibrium (labeled EQ_4 in this paper) to the stable.

We review plane Couette flow in § 2 and its symmetries in § 3. The main advance reported in this paper is the determination of a number of new moderate-Re plane Couette flow equilibria and traveling waves (§ 4), as well as explorations of the Re (§ 5) and spanwise cell aspect dependence (§ 6) of these solutions. Outstanding challenges are discussed in § 7. Detailed numerical results such as stability eigenvalues and symmetries of corresponding eigenfunctions are given in Halcrow (2008), while the complete data sets for the invariant solutions can be downloaded from `channelflow.org`.

2. Plane Couette flow – a review

Plane Couette flow is comprised of an incompressible viscous fluid confined between two infinite parallel plates moving in opposite directions at constant and equal velocities, with no-slip boundary conditions imposed at the walls. The plates move along in the streamwise or x direction, the wall-normal direction is y, and the spanwise direction is z. The fluid velocity field is $\mathbf{u}(\mathbf{x}) = [u, v, w](x, y, z)$. We define the Reynolds number as $\mathrm{Re} = Uh/\nu$, where U is half the relative velocity of the plates, h is half the distance between the plates, and ν is the kinematic viscosity. After non-dimensionalization, the plates are positioned at $y = \pm 1$ and move with velocities $\mathbf{u} = \pm 1\,\hat{\mathbf{x}}$, and the Navier-Stokes

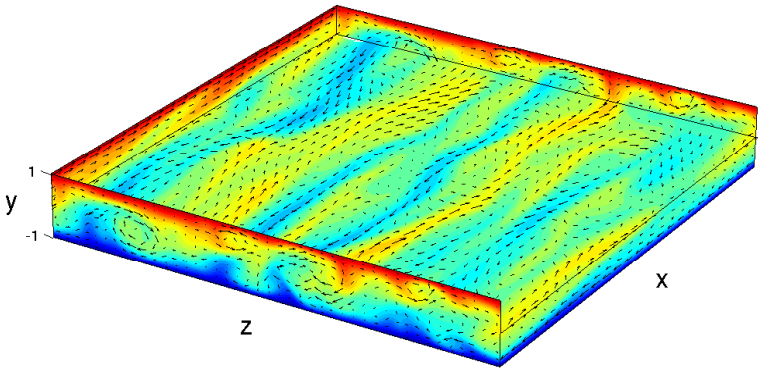

FIGURE 2. A snapshot of a typical turbulent state in a large aspect cell $[L_x, 2, L_z] = [15, 2, 15]$, $Re = 400$. The walls at $y = \pm 1$ move away/towards the viewer at equal and opposite velocities $U = \pm 1$. The color indicates the streamwise (u, or x direction) velocity of the fluid: red shows fluid moving at $u = +1$, blue, at $u = -1$. The colormap as a function of u is indicated by the laminar equilibrium in figure 4. Arrows indicate in-plane velocity in the respective planes: $[v, w]$ in (y, z) planes, etc. The top half of the fluid is cut away to show the $[u, w]$ velocity in the $y = 0$ midplane. See Gibson (2008*b*) for movies of the time evolution of such states.

equations are

$$\frac{\partial \mathbf{u}}{\partial t} + \mathbf{u} \cdot \nabla \mathbf{u} = -\nabla \mathbf{p} + \frac{\mathbf{1}}{Re} \nabla^{\mathbf{2}} \mathbf{u}\,, \quad \nabla \cdot \mathbf{u} = \mathbf{0}\,. \tag{2.1}$$

We seek spatially periodic equilibrium and traveling-wave solutions to (2.1) for the domain $\Omega = [0, L_x] \times [-1, 1] \times [0, L_z]$ (or $\Omega = [L_x, 2, L_z]$), with periodic boundary conditions in x and z. Equivalently, the periodicity of solutions can be specified in terms of their fundamental wavenumbers α and γ. A given solution is compatible with a given domain if $\alpha = mL_x/2\pi$ and $\gamma = nL_z/2\pi$ for integer m, n. In this study the spatial mean of the pressure gradient is held fixed at zero.

Most of this study is conducted at $Re = 400$ in one of the two small aspect-ratio cells:

$$\begin{aligned} \Omega_{\text{W03}} &= [2\pi/1.14, 2, 2\pi/2.5] \quad &&\approx [5.51, 2, 2.51] \approx [190, 68, 86] \quad \text{wall units} \\ \Omega_{\text{HKW}} &= [2\pi/1.14, 2, 2\pi/1.67] \quad &&\approx [5.51, 2, 3.76] \approx [190, 68, 128] \text{ wall units} \end{aligned} \tag{2.2}$$

where the wall units are in relation to a mean shear rate of $\langle \partial u/\partial y \rangle = 2.9$ in non-dimensionalized units computed for a large aspect ratio simulation at $Re = 400$. Empirically, at this Reynolds number the Ω_{HKW} cell sustains turbulence for arbitrarily long times (Hamilton *et al.* 1995), whereas the Ω_{W03} cell (Waleffe 2003) exhibits only short-lived transient turbulence (GHC). Unless stated otherwise, all calculations are carried out for Re $= 400$ and the Ω_{W03} cell. In the notation of this paper, the Nagata (1990) solutions have wavenumbers $(\alpha, \gamma) = (0.8, 1.5)$ and fit in the cell $[2\pi/0.8, 2, 2\pi/1.5] \approx [7.85, 2, 4.18]$.† Schmiegel (1999)'s study of plane Couette solutions and their bifurcations was conducted in the cell of size $\Omega = [4\pi, 2, 2\pi] \approx [12.57, 2, 6.28]$. We were not able to to obtain data for Schmiegel's solutions to make direct comparisons.

Although the cell aspect ratios studied in this paper are small, the $3D$ states explored by equilibria and their unstable manifolds explored here are strikingly similar to typical states in larger aspect cells, such as figure 2. Kim *et al.* (1971) observed that streamwise instabilities give rise to pairwise counter-rotating rolls whose spanwise separation is

† Note also that Reynolds number in Nagata (1990) is based on the full wall separation and the relative wall velocity, making it a factor of four larger than the Reynolds number used in this paper.

approximately 100 wall units. These rolls, in turn, generate streamwise streaks of high and low speed fluid, by convecting fluid alternately away from and towards the walls. The streaks have streamwise instabilities whose length scale is roughly twice the roll separation. These 'coherent structures' are prominent in numerical and experimental observations (see figure 2 and Gibson (2008*b*) animations), and they motivate our investigation of how equilibrium and traveling-wave solutions of Navier-Stokes change with Re and cell size.

Fluid states are characterized by their energy $E = \frac{1}{2}\|\mathbf{u}\|^2$ and energy dissipation rate $D = \|\nabla \times \mathbf{u}\|^2$, defined in terms of the inner product and norm

$$(\mathbf{u}, \mathbf{v}) = \frac{1}{V}\int_\Omega d\mathbf{x}\; \mathbf{u}\cdot\mathbf{v}\,, \quad \|\mathbf{u}\|^2 = (\mathbf{u},\mathbf{u})\,. \tag{2.3}$$

The rate of energy input is $I = 1/(L_x L_z)\int dxdz\, \partial u/\partial y$, where the integral is taken over the upper and lower walls at $y = \pm 1$. Normalization of these quantities is set so that $I = D = 1$ for laminar flow and $\dot{E} = I - D$. In some cases it is convenient to consider fields as differences from the laminar flow. We indicate such differences with hats: $\hat{\mathbf{u}} = \mathbf{u} - y\hat{\mathbf{x}}$.

3. Symmetries and isotropy subgroups

In an infinite domain and in the absence of boundary conditions, the Navier-Stokes equations are equivariant under any $3D$ translation, $3D$ rotation, and $\mathbf{x} \to -\mathbf{x}$, $\mathbf{u} \to -\mathbf{u}$ inversion through the origin (Frisch 1996). In plane Couette flow, the counter-moving walls restrict the rotation symmetry to rotation by π about the z-axis. We denote this rotation by σ_x and inversion through the origin by σ_{xz}. The σ_{xz} and σ_x symmetries generate a discrete dihedral group $D_1 \times D_1 = \{e, \sigma_x, \sigma_z, \sigma_{xz}\}$ of order 4, where

$$\begin{aligned}
\sigma_x\,[u,v,w](x,y,z) &= [-u,-v,w](-x,-y,z)\\
\sigma_z\,[u,v,w](x,y,z) &= [u,v,-w](x,y,-z)\\
\sigma_{xz}\,[u,v,w](x,y,z) &= [-u,-v,-w](-x,-y,-z)\,.
\end{aligned} \tag{3.1}$$

The subscripts on the σ symmetries thus indicate which of x, z change sign. The walls also restrict the translation symmetry to $2D$ in-plane translations. With periodic boundary conditions, these translations become the $SO(2)_x \times SO(2)_z$ continuous two-parameter group of streamwise-spanwise translations

$$\tau(\ell_x,\ell_z)[u,v,w](x,y,z) = [u,v,w](x+\ell_x, y, z+\ell_z)\,. \tag{3.2}$$

The equations of plane Couette flow are thus equivariant under the group $\Gamma = O(2)_x \times O(2)_z = D_{1,x} \ltimes SO(2)_x \times D_{1,z} \ltimes SO(2)_z$, where $\ltimes$ stands for a semi-direct product, x subscripts indicate streamwise translations and sign changes in x, y, and z subscripts indicate spanwise translations and sign changes in z.

The solutions of an equivariant system can satisfy all of the system's symmetries, a proper subgroup of them, or have no symmetry at all. For a given solution $\mathbf{u}$, the subgroup that contains all symmetries that fix $\mathbf{u}$ (that satisfy $s\mathbf{u} = \mathbf{u}$) is called the isotropy (or stabilizer) subgroup of $\mathbf{u}$. (Hoyle 2006; Marsden & Ratiu 1999; Golubitsky & Stewart 2002; Gilmore & Letellier 2007). For example, a typical turbulent trajectory $\mathbf{u}(\mathbf{x}, t)$ has no symmetry beyond the identity, so its isotropy group is $\{e\}$. At the other extreme is the laminar equilibrium, whose isotropy group is the full plane Couette symmetry group Γ.

In between, the isotropy subgroup of the Nagata equilibria and most of the equilibria

reported here is $S = \{e, s_1, s_2, s_3\}$, where

$$\begin{aligned} s_1\,[u,v,w](x,y,z) &= [u,v,-w](x+L_x/2,y,-z) \\ s_2\,[u,v,w](x,y,z) &= [-u,-v,w](-x+L_x/2,-y,z+L_z/2) \\ s_3\,[u,v,w](x,y,z) &= [-u,-v,-w](-x,-y,-z+L_z/2)\,. \end{aligned} \tag{3.3}$$

These particular combinations of flips and shifts match the symmetries of instabilities of streamwise-constant streaky flow (Waleffe 1997, 2003) and are well suited to the wavy streamwise streaks observable in figure 2, with suitable choice of L_x and L_z. But S is one choice among a number of intermediate isotropy groups of Γ, and other subgroups might also play an important role in the turbulent dynamics. In this section we provide a partial classification of the isotropy groups of Γ, sufficient to classify all currently known invariant solutions and to guide the search for new solutions with other symmetries. We focus on isotropy groups involving at most half-cell shifts. The main result is that among these, up to conjugacy in spatial translation, there are only five isotropy groups in which we should expect to find equilibria.

3.1. *Flips and half-shifts*

A few observations will be useful in what follows. First, we note the key role played by the inversion and rotation symmetries σ_x and σ_z (3.1) in the classification of solutions and their isotropy groups. The equivariance of plane Couette flow under continuous translations allows for traveling-wave solutions, i.e., solutions that are steady in a frame moving with a constant velocity in $[x,z]$. In state space, traveling waves either trace out circles or wind around tori, and these sets are both continuous-translation and time invariant. The sign changes under σ_x, σ_z, and σ_{xz}, however, imply particular centers of symmetry in x, z, and both x and z, respectively, and thus fix the translational phases of fields that are fixed by these symmetries. Thus the presence of σ_x or σ_z in an isotropy group prohibits traveling waves in x or z, and the presence of σ_{xz} prohibits any form of traveling wave. Guided by this observation, we will seek equilibria only for isotropy subgroups that contain the σ_{xz} inversion symmetry.

Second, the periodic boundary conditions impose discrete translation symmetries of $\tau(L_x,0)$ and $\tau(0,L_z)$ on velocity fields. In addition to this full-period translation symmetry, a solution can also be fixed under a rational translation, such as $\tau(mL_x/n,0)$ or a continuous translation $\tau(\ell_x,0)$. If a field is fixed under continuous translation, it is constant along the given spatial variable. If it is fixed under rational translation $\tau(mL_x/n,0)$, it is fixed under $\tau(mL_x/n,0)$ for $m \in [1,n-1]$ as well, provided that m and n are relatively prime. For this reason the subgroups of the continuous translation $SO(2)_x$ consist of the discrete cyclic groups $C_{n,x}$ for $n = 2,3,4,\ldots$ together with the trivial subgroup $\{e\}$ and the full group $SO(2)_x$ itself, and similarly for z. For rational shifts $\ell_x/L_x = m/n$ we simplify the notation a bit by rewriting (3.2) as

$$\tau_x^{m/n} = \tau(mL_x/n,0)\,,\ \tau_z^{m/n} = \tau(0,mL_z/n)\,. \tag{3.4}$$

Since $m/n = 1/2$ will loom large in what follows, we omit exponents of $1/2$:

$$\tau_x = \tau_x^{1/2}\,,\ \tau_z = \tau_z^{1/2}\,,\ \tau_{xz} = \tau_x\tau_z\,. \tag{3.5}$$

If a field $\mathbf{u}$ is fixed under a rational shift $\tau(L_x/n)$, it is periodic on the smaller spatial domain $x \in [0,L_x/n]$. For this reason we can exclude from our searches all equilibrium whose isotropy subgroups contain rational translations in favor of equilibria computed on smaller domains. However, as we need to study bifurcations into states with wavelengths longer than the initial state, the linear stability computations need to be carried out

in the full $[L_x, 2, L_z]$ cell. For example, if EQ is an equilibrium solution in the $\Omega_{1/3} = [L_x/3, 2, L_z]$ cell, we refer to the same solution repeated thrice in $\Omega = [L_x, 2, L_z]$ as "spanwise-tripled" or $3 \times$ EQ. Such solution is by construction fixed under the $C_{3,x} = \{e, \tau_x^{1/3}, \tau_x^{2/3}\}$ subgroup.

Third, some isotropy groups are conjugate to each other under symmetries of the full group Γ. Subgroup S' is conjugate to S if there is an $s \in \Gamma$ for which $S' = s^{-1}Ss$. In spatial terms, two conjugate isotropy groups are equivalent to each other under a coordinate transformation. A set of conjugate isotropy groups forms a conjugacy class. It is necessary to consider only a single representative of each conjugacy class; solutions belonging to conjugate isotropy groups can be generated by applying the symmetry operation of the conjugacy.

In the present case conjugacies under spatial translation symmetries are particularly important. Note that $O(2)$ is not an abelian group, since reflections σ and translations τ along the same axis do not commute (Harter 1993). Instead we have $\sigma\tau = \tau^{-1}\sigma$. Rewriting this relation as $\sigma\tau^2 = \tau^{-1}\sigma\tau$, we note that

$$\sigma_x\tau_x(\ell_x, 0) = \tau^{-1}(\ell_x/2, 0)\,\sigma_x\,\tau(\ell_x/2, 0)\,. \tag{3.6}$$

The right-hand side of (3.6) is a similarity transformation that translates the origin of coordinate system. For $\ell_x = L_x/2$ we have

$$\tau_x^{-1/4}\,\sigma_x\,\tau_x^{1/4} = \sigma_x\tau_x\,, \tag{3.7}$$

and similarly for the spanwise shifts / reflections. Thus for each isotropy group containing the shift-reflect $\sigma_x\tau_x$ symmetry, there is a simpler conjugate isotropy group in which $\sigma_x\tau_x$ is replaced by σ_x (and similarly for $\sigma_z\tau_z$ and σ_z). We choose as the representative of each conjugacy class the simplest isotropy group, in which all such reductions have been made. However, if an isotropy group contains both σ_x and $\sigma_x\tau_x$, it cannot be simplified this way, since the conjugacy simply interchanges the elements.

Fourth, for $\ell_x = L_x$, we have $\tau_x^{-1}\,\sigma_x\,\tau_x = \sigma_x$, so that, in the special case of half-cell shifts, σ_x and τ_x commute. For the same reason, σ_z and τ_z commute, so the order-16 isotropy subgroup

$$G = D_{1,x} \times C_{2,x} \times D_{1,z} \times C_{2,z} \subset \Gamma \tag{3.8}$$

is abelian.

3.2. *The 67-fold path*

We now undertake a partial classification of the lattice of isotropy subgroups of plane Couette flow. We focus on isotropy groups involving at most half-cell shifts, with $SO(2)_x \times SO(2)_z$ translations restricted to order 4 subgroup of spanwise-streamwise translations (3.5) of half the cell length,

$$T = C_{2,x} \times C_{2,z} = \{e, \tau_x, \tau_z, \tau_{xz}\}\,. \tag{3.9}$$

All such isotropy subgroups of Γ are contained in the subgroup G (3.8). Within G, we look for the simplest representative of each conjugacy class, as described above.

Let us first enumerate all subgroups $H \subset G$. The subgroups can be of order $|H| = \{1, 2, 4, 8, 16\}$. A subgroup is generated by multiplication of a set of generator elements, with the choice of generator elements unique up to a permutation of subgroup elements. A subgroup of order $|H| = 2$ has only one generator, since every group element is its own inverse. There are 15 non-identity elements in G to choose from, so there are 15 subgroups of order 2. Subgroups of order 4 are generated by multiplication of two group elements. There are 15 choices for the first and 14 choices for the second. However, each order-4

subgroup can be generated by $3 \cdot 2$ different choices of generators. For example, any two of $\tau_x, \tau_z, \tau_{xz}$ in any order generate the same group T. Thus there are $(15 \cdot 14)/(3 \cdot 2) = 35$ subgroups of order 4.

Subgroups of order 8 have three generators. There are 15 choices for the first generator, 14 for the second, and 12 for the third. There are 12 choices for the third generator and not 13, since if it were chosen to be the product of the first two generators, we would get a subgroup of order 4. Each order-8 subgroup can be generated by $7 \cdot 6 \cdot 4$ different choices of three generators, so there are $(15 \cdot 14 \cdot 12)/(7 \cdot 6 \cdot 4) = 15$ subgroups of order 8. In summary: there is the group G itself, of order 16, 15 subgroups of order 8, 35 of order 4, 15 of order 2, and 1 (the identity) of order 1, or 67 subgroups in all (Halcrow 2008). This is whole lot of isotropy subgroups to juggle; fortunately, the observations of § 3.1 show that there are only 5 *distinct conjugacy classes* in which we can expect to find equilibria.

The 15 order-2 groups fall into 8 distinct conjugacy classes, under conjugacies between $\sigma_x\tau_x$ and σ_x and $\sigma_z\tau_z$ and σ_z. These conjugacy classes are represented by the 8 isotropy groups generated individually by the 8 generators σ_x, σ_z, σ_{xz}, $\sigma_x\tau_z$, $\sigma_z\tau_x$, τ_x, τ_z, and τ_{xz}. Of these, the latter three imply periodicity on smaller domains. Of the remaining five, σ_x and $\sigma_x\tau_z$ allow traveling waves in z, σ_z and $\sigma_z\tau_x$ allow traveling waves in x. Only a single conjugacy class, represented by the isotropy group

$$\{e, \sigma_{xz}\}, \tag{3.10}$$

breaks both continuous translation symmetries. Thus, of all order-2 isotropy groups, we expect only this group to have equilibria. EQ_9, EQ_{10}, and EQ_{11} described below are examples of equilibria with isotropy group $\{e, \sigma_{xz}\}$.

Of the 35 subgroups of order 4, we need to identify those that contain σ_{xz} and thus support equilibria. We choose as the simplest representative of each conjugacy class the isotropy group in which σ_{xz} appears in isolation. Four isotropy subgroups of order 4 are generated by picking σ_{xz} as the first generator, and σ_z, $\sigma_z\tau_x$, $\sigma_z\tau_z$, or $\sigma_z\tau_{xz}$ as the second generator (R for reflect-rotate):

$$\begin{aligned}
R &= \{e, \sigma_x, \sigma_z, \sigma_{xz}\} &&= \{e, \sigma_{xz}\} \times \{e, \sigma_z\} \\
R_x &= \{e, \sigma_x\tau_x, \sigma_z\tau_x, \sigma_{xz}\} &&= \{e, \sigma_{xz}\} \times \{e, \sigma_x\tau_x\} \\
R_z &= \{e, \sigma_x\tau_z, \sigma_z\tau_z, \sigma_{xz}\} &&= \{e, \sigma_{xz}\} \times \{e, \sigma_z\tau_z\} \\
R_{xz} &= \{e, \sigma_x\tau_{xz}, \sigma_z\tau_{xz}, \sigma_{xz}\} &&= \{e, \sigma_{xz}\} \times \{e, \sigma_z\tau_{xz}\} \simeq S\,.
\end{aligned} \tag{3.11}$$

These are the only isotropy groups of order 4 containing σ_{xz} and no isolated translation elements. Together with $\{e, \sigma_{xz}\}$, these 5 isotropy subgroups represent the 5 conjugacy classes in which expect to find equilibria.

The R_{xz} isotropy subgroup is particularly important, as the Nagata (1990) equilibria belong to this conjugacy class (Waleffe 1997; Clever & Busse 1997; Waleffe 2003), as do most of the solutions reported here. The *NBC* isotropy subgroup of Schmiegel (1999) and S of Gibson *et al.* (2008*b*) are conjugate to R_{xz} under quarter-cell coordinate transformations. In keeping with previous literature, we often represent this conjugacy class with $S = \{e, s_1, s_2, s_3\} = \{e, \sigma_z\tau_x, \sigma_x\tau_{xz}, \sigma_{xz}\tau_z\}$ rather than the simpler conjugate group R_{xz}. Schmiegel's I isotropy group is conjugate to our R_z; Schmiegel (1999) contains many examples of R_z-isotropic equilibria. R-isotropic equilibria were found by Tuckerman & Barkley (2002) for plane Couette flow in which the translation symmetries were broken by a streamwise ribbon. We have not searched for R_x-isotropic solutions, and are not aware of any published in the literature.

The remaining subgroups of orders 4 and 8 all involve $\{e, \tau_i\}$ factors and thus involve

states that are periodic on half-domains. For example, the isotropy subgroup of EQ_7 and EQ_8 studied below is $S \times \{e, \tau_{xz}\} \simeq R \times \{e, \tau_{xz}\}$, and thus these are doubled states of solutions on half-domains. For the detailed count of all 67 subgroups, see Halcrow (2008).

3.3. *State-space visualization*

GHC presents a method for visualizing low-dimensional projections of trajectories in the infinite-dimensional state space of the Navier-Stokes equations. Briefly, we construct an orthonormal basis $\{\mathbf{e}_1, \mathbf{e}_2, \cdots, \mathbf{e}_n\}$ that spans a set of physically important fluid states $\hat{\mathbf{u}}_A$, $\hat{\mathbf{u}}_B$, ..., such as equilibrium states and their eigenvectors, and we project the evolving fluid state $\hat{\mathbf{u}}(t) = \mathbf{u} - y\hat{\mathbf{x}}$ onto this basis using the L^2 inner product (2.3). It is convenient to use differences from laminar flow, since $\hat{\mathbf{u}}$ forms a vector space with the laminar equilibrium at the origin, closed under addition. This produces a low-dimensional projection

$$a(t) = (a_1, a_2, \cdots, a_n, \cdots)(t)\,, \qquad a_n(t) = (\hat{\mathbf{u}}(t), \mathbf{e}_n)\,, \tag{3.12}$$

which can be viewed in $2d$ planes $\{\mathbf{e}_m, \mathbf{e}_n\}$ or in $3d$ perspective views $\{\mathbf{e}_\ell, \mathbf{e}_m, \mathbf{e}_n\}$. The state-space portraits are *dynamically intrinsic*, since the projections are defined in terms of intrinsic solutions of the equations of motion, and *representation independent*, since the inner product (2.3) projection is independent of the numerical or experimental representation of the fluid state data. Such bases are effective because moderate-Re turbulence explores a small repertoire of unstable coherent structures (rolls, streaks, their mergers), so that the trajectory $a(t)$ does not stray far from the subspace spanned by the key structures.

There is no *a priori* prescription for picking a 'good' set of basis fluid states, and construction of $\{\mathbf{e}_n\}$ set requires some experimentation. Let the S-invariant subspace be the flow-invariant subspace of states $\mathbf{u}$ that are fixed under S; this consists of all states whose isotropy group is S or contains S as a subgroup. The plane Couette system at hand has a total of 29 known equilibria within the S-invariant subspace four translated copies each of EQ_1 - EQ_6, two translated copies of EQ_7 (which have an additional τ_{xz} symmetry), plus the laminar equilibrium EQ_0 at the origin. As shown in GHC, the dynamics of different regions of state space can be elucidated by projections onto basis sets constructed from combinations of equilibria and their eigenvectors.

In this paper we present global views of all invariant solutions in terms of the orthonormal 'translational basis' constructed in GHC from the four translated copies of EQ_2:

$$\begin{array}{lccc} & \tau_x & \tau_z & \tau_{xz} \\ \mathbf{e}_1 = c_1(1 + \tau_x + \tau_z + \tau_{xz})\,\hat{\mathbf{u}}_{\mathrm{EQ}2} & + & + & + \\ \mathbf{e}_2 = c_2(1 + \tau_x - \tau_z - \tau_{xz})\,\hat{\mathbf{u}}_{\mathrm{EQ}2} & + & - & - \\ \mathbf{e}_3 = c_3(1 - \tau_x + \tau_z - \tau_{xz})\,\hat{\mathbf{u}}_{\mathrm{EQ}2} & - & + & - \\ \mathbf{e}_4 = c_4(1 - \tau_x - \tau_z + \tau_{xz})\,\hat{\mathbf{u}}_{\mathrm{EQ}2} & - & - & +\,, \end{array} \tag{3.13}$$

where c_n is a normalization constant determined by $\|\mathbf{e}_n\| = 1$. The last 3 columns indicate the symmetry of the basis vector under half-cell translations; e.g. ± 1 in the τ_x column implies $\tau_x \mathbf{e}_j = \pm \mathbf{e}_j$.

4. Equilibria and traveling waves of plane Couette flow

We seek equilibrium solutions to (2.1) of the form $\mathbf{u}(\mathbf{x}, t) = \mathbf{u}_{\mathrm{EQ}}(\mathbf{x})$ and traveling-wave or relative equilibrium solutions of the form $\mathbf{u}(\mathbf{x}, t) = \mathbf{u}_{\mathrm{TW}}(\mathbf{x} - \mathbf{c}t)$ with $\mathbf{c} = (c_x, 0, c_z)$.

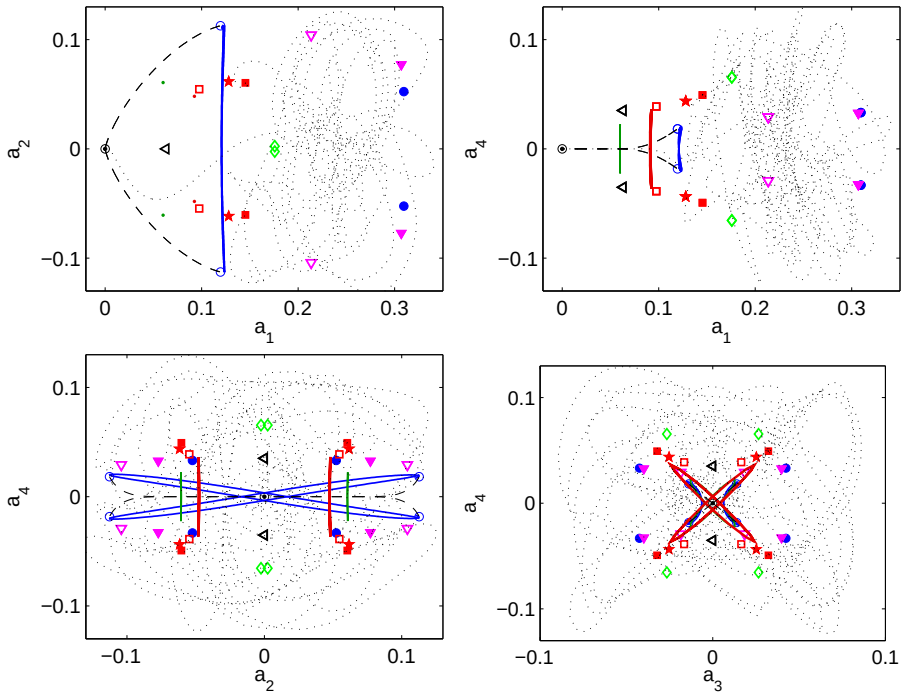

FIGURE 3. Four projections of equilibria, traveling waves and their half-cell shifts onto translational basis (3.13) constructed from equilibrium EQ_4. Equilibria are marked $\odot$ EQ_0, $\circ$ EQ_1, $\bullet$ EQ_2, $\square$ EQ_3, $\blacksquare$ EQ_4, $\lozenge$ EQ_5, $\triangleleft$ EQ_7, $\bigstar$ EQ_9, $\triangledown$ EQ_{10}, and $\blacktriangledown$ EQ_{11}. Traveling waves trace out closed loops. In some projections the loops appear as line segments or points. TW_1(blue) is a spanwise-traveling, symmetry-breaking bifurcation off EQ_1, so it passes close to different translational phases of $\circ$ EQ_1. Similarly, TW_3 (red) bifurcates off $\square$ EQ_3 and so passes near its translations. TW_2 (green) was not discovered through bifurcation (see § 4); it appears as the shorter, isolated line segment in (a_1, a_4) and (a_2, a_4). The $\mathrm{EQ}_1 \to \mathrm{EQ}_0$ relaminarizing heteroclinic connections are marked by dashed lines. A long-lived transiently turbulent trajectory is plotted with a dotted line. The EQ_4-translational basis was chosen here since it displays the shape of traveling waves more clearly than the projection on the EQ_2-translational basis of figure 1.

Let $\mathbf{F}_{\mathrm{NS}}(\mathbf{u})$ represent the Navier-Stokes equations (2.1) for the given geometry, boundary conditions, and Reynolds number, and $\mathbf{f}^t_{\mathrm{NS}}$ its time-t forward map

$$\frac{\partial \mathbf{u}}{\partial t} = \mathbf{F}_{\mathrm{NS}}(\mathbf{u})\,, \qquad \mathbf{f}^t_{\mathrm{NS}}(\mathbf{u}) = \mathbf{u} + \int_0^t d\tau\, \mathbf{F}_{\mathrm{NS}}(\mathbf{u})\,. \tag{4.1}$$

Then for any fixed $T > 0$, equilibria satisfy $\mathbf{f}^T(\mathbf{u}) - \mathbf{u} = 0$ and traveling waves satisfy $\mathbf{f}^T(\mathbf{u}) - \tau\,\mathbf{u} = 0$, where $\tau = \tau(c_x T, c_z T)$. When $\mathbf{u}$ is approximated with a finite spectral expansion and $\mathbf{f}^t$ with CFD algorithm, these equations become set of nonlinear equations in the expansion coefficients for $\mathbf{u}$ and, in the case of traveling waves, the wave velocities $(c_x, 0, c_z)$.

Viswanath (2007) presents an algorithm for computing solutions to these equations based on Newton search, Krylov subspace methods, and an adaptive 'hookstep' trust-region limitation to the Newton steps. This algorithm can provide highly accurate solutions from even poor initial guesses. The high accuracy stems from the use of Krylov subspace methods, which can be efficient with 10^5 or more spectral expansion coefficients. The robustness with respect to initial guess stems from the hookstep algorithm.

The hookstep limitation restricts steps to a radius r of estimated validity for the local linear approximation to the Newton equations. As r increases from zero, the hookstep varies smoothly from the Krylov-subspace gradient direction to the Newton step, so that the hookstep algorithm behaves as a gradient descent when far away from a solution and as the Newton method when near, thus greatly increasing the algorithm's region of convergence around solutions, compared to the Newton method (J.E. Dennis, Jr., & Schnabel 1996).

The choice of initial guesses for the search algorithm is one of the main differences between this study and previous calculations of equilibria and traveling waves of shear flows. Prior studies have used homotopy, that is, starting from a solution to a closely related problem and following it through small steps in parameter space to the problem of interest. Equilibria for plane Couette flow have been continued from Taylor-Couette flow (Nagata 1990), Rayleigh-Bénard flow (Clever & Busse 1997), and from plane Couette with imposed body forces (Waleffe 1997). Equilibria and traveling waves have also been found using "edge-tracking" algorithms, that is, by adjusting the magnitude of a perturbation of the laminar flow until it neither decays to laminar nor grows to turbulence, but instead converges toward a nearby weakly unstable solution (Skufca *et al.* (2006); Viswanath (2008); Schneider *et al.* (2008)). In this study, we take as initial guesses samples of velocity fields generated by long-time simulations of turbulent dynamics. The intent is to find the *dynamically most important* solutions, by sampling the turbulent flow's natural measure.

We discretize $\mathbf{u}$ with a spectral expansion of the form

$$\mathbf{u}(\mathbf{x}) = \sum_{j=-J}^{J} \sum_{k=-K}^{K} \sum_{\ell=0}^{L} \sum_{m=1}^{3} \mathbf{u}_{jkl}\, T_\ell(y)\, e^{2\pi i(jx/L_x + kz/L_z)}\,, \tag{4.2}$$

where the T_ℓ are Chebyshev polynomials. Time integration of $\mathbf{f}^t$ is performed with a primitive-variables Chebyshev-tau algorithm with tau correction, influence-matrix enforcement of boundary conditions, and third-order backwards differentiation time stepping, and dealiasing in x and z (Kleiser & Schuman (1980); Canuto *et al.* (1988); Peyret (2002)). We eliminate from the search space the linearly dependent spectral coefficients of $\mathbf{u}$ that arise from incompressibility, boundary conditions, and complex conjugacies that arise from the real-valuedness of velocity fields. Our Navier-Stokes integrator, implementation of the Newton-hookstep search algorithm, and all solutions described in this paper are available for download from `channelflow.org` website (Gibson 2008*a*). For further details on the numerical methods see GHC and Halcrow (2008).

Solutions presented in this paper use spatial discretization (4.2) with $(J, K, L) = (15, 15, 32)$ (or $32\times33\times32$ gridpoints) and roughly 60k expansion coefficients. The estimated accuracy of each solution is listed in table 1. As is clear from Schmiegel (1999) Ph.D. thesis, ours is almost certainly an incomplete inventory; while for any finite Re, finite-aspect ratio cell the number of distinct equilibrium and traveling wave solutions is finite, we know of no way of determining or bounding this number. It is difficult to compare our solutions directly to those of Schmiegel since those solutions were computed in a $[4\pi, 2, 2\pi]$ cell (roughly twice our cell size in both span and streamwise directions) and with lower spatial resolution (2212 independent expansion functions versus our 60k for a cell of one-fourth the volume). We expect that many of Schmiegel's equilibria could be continued to higher resolution and smaller cells.

4.1. *Equilibrium solutions*

Our primary focus is on the S-invariant subspace (3.3) of the Ω_{W03} cell at $Re = 400$. We initiated 28 equilibrium searches at evenly spaced intervals $\Delta t = 25$ along a trajectory in the unstable manifold of EQ_4 that exhibited turbulent dynamics for 800 nondimensionalized time units after leaving the neighborhood of EQ_4 and before decaying to laminar flow. The solutions are numbered in order of discovery, adjusted so that lower, upper branch solutions are labeled with consecutive numbers. EQ_0 is the laminar equilibrium, EQ_1 and EQ_2 are the Nagata lower and upper branch, and EQ_4 is the $\mathbf{u}_{\text{NB}}$ solution reported in GHC. The rest are new. Only one of the 28 searches failed to converge onto an equilibrium; the successful searches converged to equilibria with frequencies listed in table 1. The higher frequency of occurrence of EQ_1 and EQ_4 suggests that these are the dynamically most important equilibria in the S-invariant subspace for the Ω_{W03} cell at $Re = 400$. Stability eigenvalues of known equilibria are plotted in figure 7. Tables of stability eigenvalues and other properties of these solutions are given in Halcrow (2008), while the images, movies and full data sets are available online at `channelflow.org`. All equilibrium solutions have zero spatial-mean pressure gradient, which was imposed in the flow conditions, and, due to their symmetry, zero mean velocity.

EQ_1, EQ_2 equilibria. This pair of solutions was discovered by Nagata (1990), recomputed by different methods by Clever & Busse (1997) and Waleffe (1998, 2003), and found multiple times in randomly initiated searches as described above. The lower branch EQ_1 and the upper branch EQ_2 are born together in a saddle-node bifurcation at $Re \approx 218.5$. Just above bifurcation, the two equilibria are connected by a $\text{EQ}_1 \to \text{EQ}_2$ heteroclinic connection, see Halcrow *et al.* (2008). However, at higher values of Re there appears to be no such simple connection. The lower branch EQ_1 equilibrium is discussed in detail in Wang *et al.* (2007). This equilibrium has a 1-dimensional unstable manifold for a wide range of parameters. Its stable manifold appears to provide a partial barrier between the basin of attraction of the laminar state and turbulent states (Schneider *et al.* 2008). The upper branch EQ_2 has an 8-dimensional unstable manifold and a dissipation rate that is higher than the turbulent mean, see figure 8 (a). However, within the S-invariant subspace EQ_2 has just one pair of unstable complex eigenvalues. The two-dimensional S-invariant section of its unstable manifold was explored in some detail in GHC. It appears to bracket the upper end of turbulence in state space, as illustrated by figure 1.

EQ_3, EQ_4 equilibria. EQ_4 was found in GHC and is called $\mathbf{u}_{\text{NB}}$ there. Its lower-branch partner EQ_3 was found by continuing EQ_4 downwards in Re and also by independent searches from samples of turbulent data. EQ_4 is, with EQ_1, the most frequently found equilibrium, which attests to its importance in turbulent dynamics. Like EQ_1, EQ_4 serves as a gatekeeper between turbulent flow and the laminar basin of attraction. As shown in GHC, there is a heteroclinic connection from EQ_4 to EQ_1 resulting from a complex instability of EQ_4. Trajectories on one side of the heteroclinic connection decay rapidly to laminar flow; those one the other side take excursion towards turbulence.

EQ_5, EQ_6 equilibria. EQ_5 was found only once in our random searches, and its upper-branch partner EQ_6 only by continuation in Reynolds number. We were only able to continue EQ_6 up to $Re = 330$. At this value it is highly unstable, with a 19 dimensional unstable manifold, and it is far more dissipative than a typical turbulent trajectory.

EQ_7, EQ_8 equilibria. EQ_7 and EQ_8 appear together in a saddle node bifurcation in Re (see § 5). EQ_7 / EQ_8 might be the same as Schmiegel (1999)'s 'σ solutions'. The x-average velocity field plots appear very similar, as do the D versus Re bifurcation diagrams. We were not able to obtain Schmiegel's data in order to make a direct comparison. In this cell, we were not able to continue EQ_8 past $\text{Re} = 270$. EQ_7 is both the closest

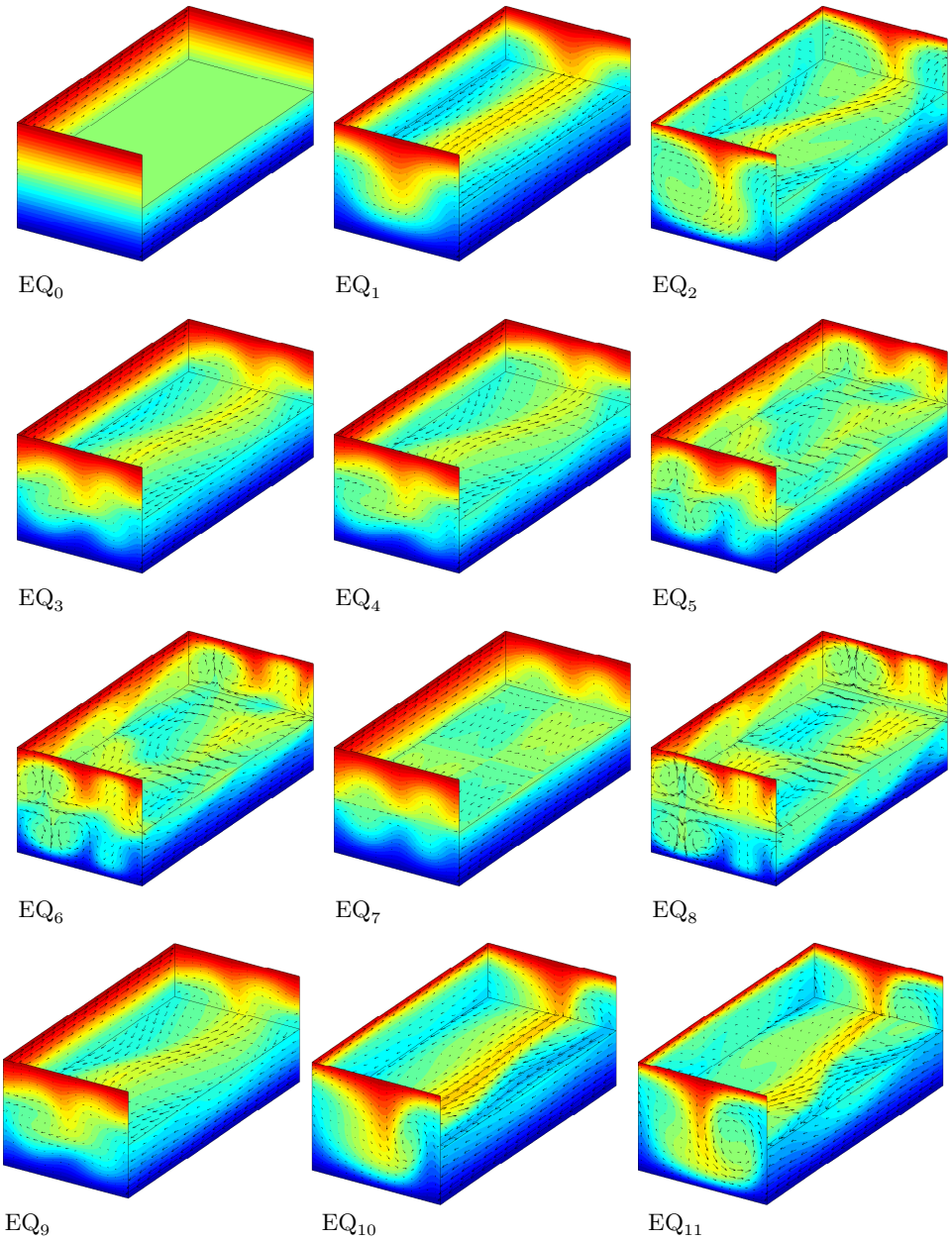

FIGURE 4. Equilibria EQ_0 (laminar solution) through EQ_{11} in Ω_{W03} cell. Plotting conventions are the same as figure 2. $Re = 400$ except for EQ_6, $Re = 330$, and EQ_8, $Re = 270$.

state to laminar in terms of disturbance energy and the lowest in terms of drag. It has one strongly unstable real eigenvalue within the S-invariant subspace and two weakly unstable eigenvalues with $\{s_1, s_3\}$ and $\{s_2, s_3\}$ antisymmetries, respectively. In this regard, the EQ7 unstable manifold might, like the unstable manifold of EQ_1, form part of the boundary between the laminar basin of attraction and turbulence. EQ_7 and EQ_8 are unique among the equilibria determined here in that they have the order-8 isotropy subgroup $S \times \{e, \tau_{xz}\}$ (see § 3.2). The action of the quotient group $G/(S \times \{e, \tau_{xz}\})$ yields

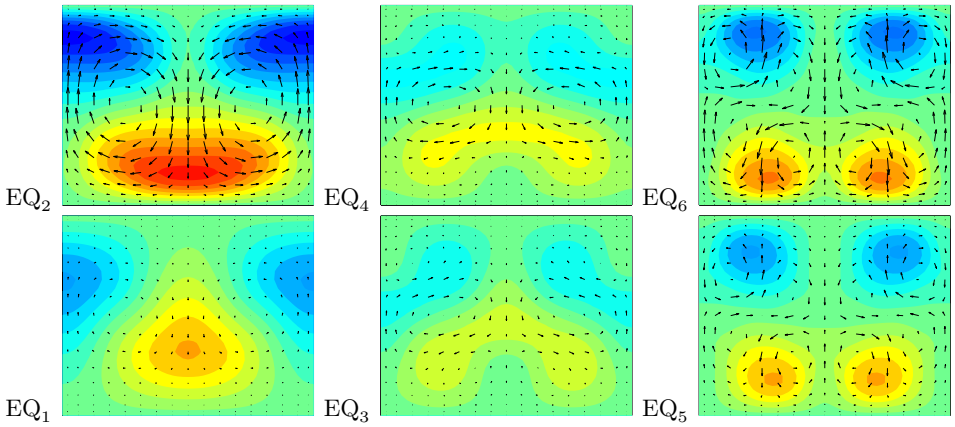

FIGURE 5. x-average of $\hat{\mathbf{u}}(y,z)$ for equilibria EQ_1-EQ_6 in Ω_{W03} cell. Arrows indicate $[\hat{v},\hat{w}]$, and the colormap indicates $\hat{u}$: red/blue is $\hat{u}=\pm 1$, green is $\hat{u}=0$. All figures have the same scaling between arrow length and magnitude of $[\hat{v},\hat{w}]$. Lower and upper-branch pairs are grouped together vertically, e.g. EQ_1, EQ_2 are a lower, upper branch pair. $Re=400$ except for $Re=330$ in EQ_6.

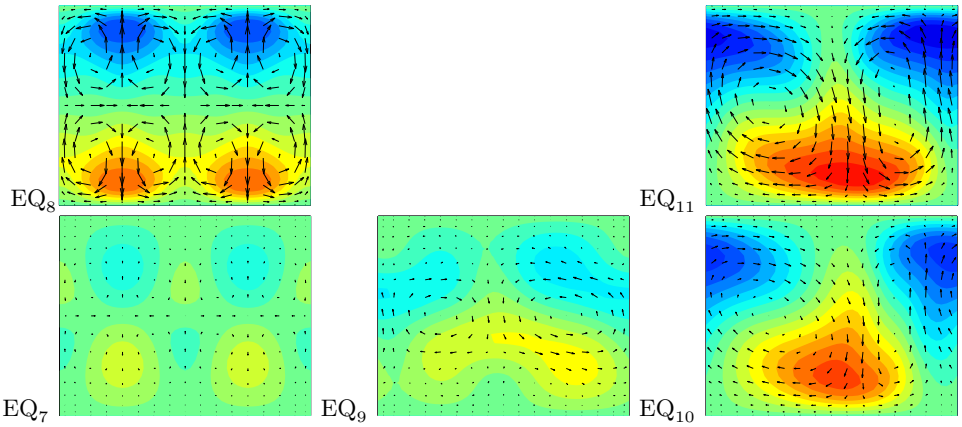

FIGURE 6. x-average of $\hat{\mathbf{u}}(y,z)$ for equilibria EQ_7-EQ_{11}. Plotting conventions are the same as in figure 5. $Re=400$ except for $Re=270$ in EQ_8.

2 copies of each, plotted in figure 3. EQ_7 and EQ_8 are similar in appearance to EQ_5 and EQ_6, except for the additional symmetry.

EQ_9 equilibrium is a single lopsided roll-streak pair. It is produced by a pitchfork bifurcation from EQ_4 at $Re\approx 370$ as an $\{s_1,s_2\}$-antisymmetric eigenfunction goes through marginal stability (the only pitchfork bifurcation we have yet found) and remains close to EQ_4 at $Re=400$. Thus, it has $\{e,\sigma_{xz}\}$ isotropy. Even though EQ_9 is not S-isotropic, we found it from a search initiated on a guess that was S-isotropic to single precision. Such small asymmetries were enough to draw the Newton-hookstep out of the S-invariant subspace.

EQ_{10} / EQ_{11} equilibria are produced in a saddle-node bifurcation at $Re\approx 348$ as a lower / upper branch pair, and they lie close to the center of mass of the turbulent repeller, see figure 8 (a). They look visually similar to typical turbulent states for this cell size. However, they are both highly unstable and unlikely to be revisited frequently by a generic turbulent fluid state. Their isotropy subgroup $\{e,\sigma_{xz}\}$ is order 2, so the action

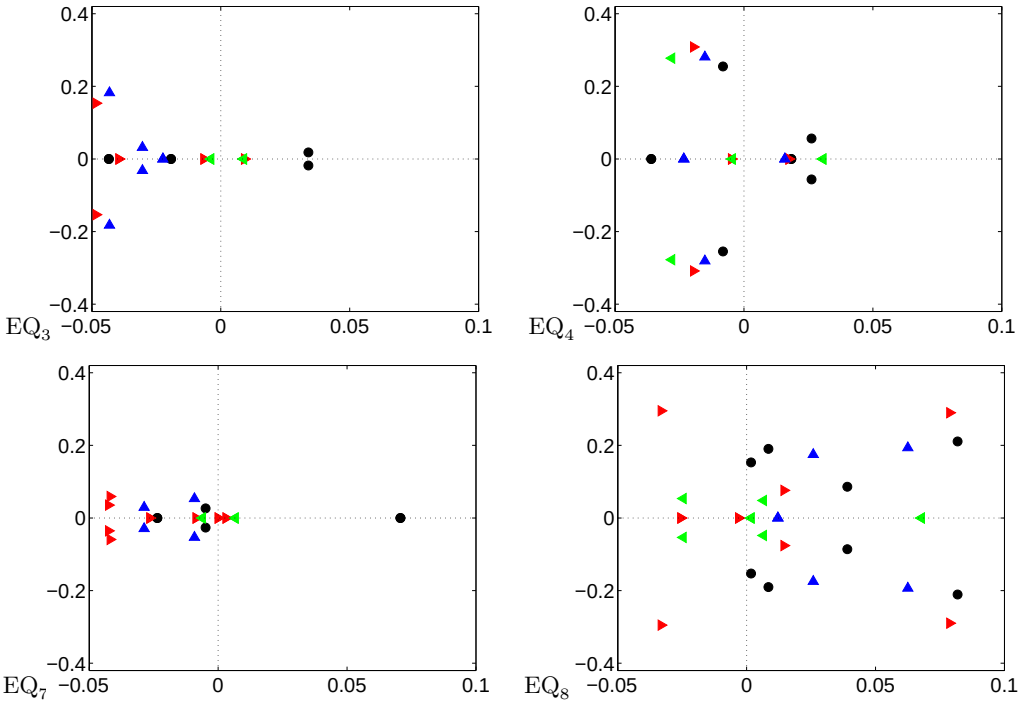

FIGURE 7. Eigenvalues of equilibria EQ_3, EQ_4 and EQ_7, EQ_8 in Ω_{W03} cell, $Re = 400$. Eigenvalues are plotted according to their symmetries: ● $+++$, the S-invariant subspace, ▶ $+--$, ◀ $-+-$, and ▲ $--+$, where $\pm$ stand symmetric/antisymmetric in s_1, s_2, and s_3 respectively. For EQ_1, EQ_2 and EQ_4 eigenvalues see GHC (there referred to as $\mathbf{u}_{\mathrm{LB}}$, $\mathbf{u}_{\mathrm{UB}}$ and $\mathbf{u}_{\mathrm{NB}}$, respectively). For numerical values of all stability eigenvalues see Halcrow (2008) and `channelflow.org`.

of the quotient group $G/\{e, \tau_{xz}\}$ yields 8 copies of each, which appear as the 4 overlaid pairs in projections onto the (3.13) basis set, see figure 1 and figure 3.

4.2. *Traveling waves*

The first two traveling-wave solutions reported in the literature were found by Nagata (1997) by continuing EQ_1 equilibrium to a combined Couette / Poiseuille channel flow, and then continuing back to plane Couette flow. The result was a pair of streamwise traveling waves arising from a saddle-node bifurcation. Viswanath (2008) found two traveling waves, 'D1' and the same solution 'D2,' but at a higher $Re = 1000$, through an edge-tracking algorithm (Skufca *et al.* (2006), see also § 4.1). Here we verify Viswanath's solution and present two new traveling-wave solutions computed as symmetry-breaking bifurcations off equilibrium solutions. We were not able to compare these to Nagata's traveling waves since the data is not available. The traveling waves are shown as 3D velocity fields in figure 9 and as closed orbits in state space in figure 3. Their kinetic energies and dissipation rates are tabulated in table 1. Each traveling-wave solution has a zero spatial-mean pressure gradient but non-zero mean velocity in the same direction as the wave velocity. It is likely each solution could be continued to zero wave velocity but non-zero spatial-mean pressure gradient.

$\mathbf{TW}_1$ traveling wave is s_2-isotropic and hence spanwise traveling. At $Re = 400$ its velocity is very small, $\mathbf{c} = 0.00655\ \hat{\mathbf{z}}$, and it has a small but nonzero mean velocity, also in the spanwise direction. This is a curious property: TW_1 induces bulk transport of fluid without a pressure gradient, and in a direction orthogonal to the motion of the

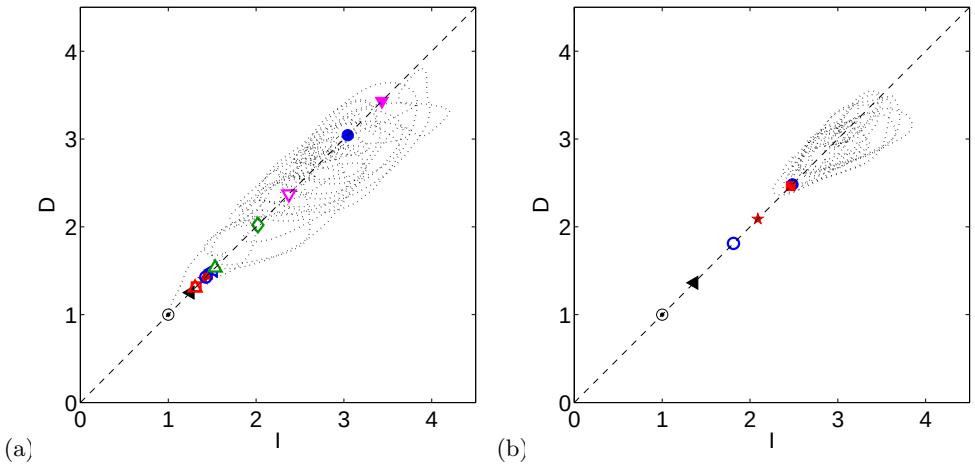

FIGURE 8. Rate of energy input at the walls I versus dissipation D, for the known equilibria and traveling waves in (a) $\Omega_{\rm W03}$ (b) $\Omega_{\rm HKW}$ cell at $Re = 400$. $\odot$ $\mathrm{EQ}_0$is the laminar equilibrium with $D = I = 1$. In (a), $\circ$ EQ_1, $\square$ EQ_3, $\blacksquare$ EQ_4, $\triangleleft$ EQ_7, $\bigstar$ EQ_9, $\triangleright$ TW_1, $\triangle$ TW_2, and $\triangle$ TW_3 are clustered in the range $1.25 < D = I < 1.55$, and $\bullet$ EQ_2, $\diamond$ EQ_5, $\triangledown$ EQ_{10}, and $\blacktriangledown$ EQ_{11} lie in $2 < D = I < 4$. In (b), the symbols are the same, and $\blacksquare$ EQ_4, $\bullet$ EQ_2 are clustered together near $D = I \approx 2.47$.

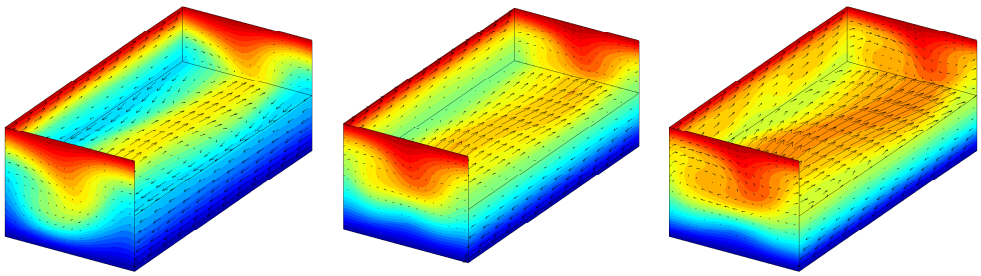

FIGURE 9. Spanwise TW_1, streamwise TW_2 and TW_3 traveling waves in $\Omega_{\rm W03}$ cell, $Re = 400$.

walls. TW_1 was found as a pitchfork bifurcation from EQ_1, and thus lies very close to it in state space. It is weakly unstable, with a $3D$ unstable manifold with two eigenvalues which are extremely close to marginal. In this sense TW_1 unstable manifold is nearly one-dimensional, and comparable to EQ_1.

TW$_2$ is a streamwise traveling wave found by Viswanath (2008) and called D1 there. It is s_1-isotropic, has a low dissipation rate, and a small but nonzero mean velocity in the streamwise direction. Viswanath provided data for this solution; we verified it with an independent numerical integrator and continued the solution to $\Omega_{\rm W03}$ cell for comparison with the other traveling waves. In this cell TW_2 is fairly stable, with an eigenspectrum similar to TW_1's, except with different symmetries.

TW$_3$ is an s_1-isotropic streamwise traveling wave with a relatively high wave velocity $\mathbf{c} = 0.465\ \hat{\mathbf{x}}$ and a nonzero mean velocity in the streamwise direction. Its dissipation rate and energy norm are close to those of TW_1.

	Re	$\|\cdot\|$	E	D	H	$\dim W^u$	$\dim W^u_H$	acc.	freq.
mean		0.2828	0.087	2.926					
EQ_0		0	0.1667	1	Γ	0	0		2
EQ_1		0.2091	0.1363	1.429	S	1	1	10^{-6}	7
EQ_2		0.3858	0.0780	3.044	S	8	2	10^{-4}	3
EQ_3		0.1259	0.1382	1.318	S	4	2	10^{-4}	2
EQ_4		0.1681	0.1243	1.454	S	6	3	10^{-4}	8
EQ_5		0.2186	0.1073	2.020	S	11	4	10^{-3}	1
EQ_6	330	0.2751	0.0972	2.818	S	19	6	10^{-3}	
EQ_7		0.0935	0.1469	1.252	$S \times \{e, \tau_{xz}\}$	3	1	10^{-4}	3
EQ_8	270	0.3466	0.0853	3.672	$S \times \{e, \tau_{xz}\}$	21	8	10^{-4}	
EQ_9		0.1565	0.1290	1.404	$\{e, \sigma_{xz}\}$	5		10^{-4}	1
EQ_{10}		0.3285	0.1080	2.373	$\{e, \sigma_{xz}\}$	10		10^{-4}	
EQ_{11}		0.4049	0.0803	3.432	$\{e, \sigma_{xz}\}$	13		10^{-4}	

TABLE 1. Properties of equilibrium solutions for Ω_{W03} cell, $Re = 400$, unless noted otherwise. The mean values are ensemble and time averages over transient turbulence. $\|\cdot\|$ is the L^2-norm of the velocity deviation from laminar, E is the energy density (2.3), D is the dissipation rate, H is the isotropy subgroup, $\dim W^u$ is the dimension of the equilibrium's unstable manifold or the number of its unstable eigenvalues, and $\dim W^u_H$ is the dimensionality of the unstable manifold within the H-invariant subspace, or the number of unstable eigenvalues with the same symmetries as the equilibrium. The accuracy *acc.* of the solution at a given resolution (a $32 \times 33 \times 32$ grid) is estimated by the magnitude of the residual $\|(f^{T=1}(\mathbf{u}) - \mathbf{u})\|/\|\mathbf{u}\|$ when the solution is interpolated and integrated at higher resolution (a $48 \times 49 \times 48$ grid). The *freq.* column shows how many times a solution was found among the 28 searches initiated with samples of the natural measure within within the S-invariant subspace. See also figure 8 (a).

	$\|\cdot\|$	E	D	H	$\dim W^u$	$\dim W^u_H$	$\mathbf{c}$	mean $\mathbf{u}$
mean	0.2828	0.087	2.926					
TW_1	0.2214	0.1341	1.510	$\{e, \sigma_x\tau_z\}$	3	2	0.00655 $\hat{\mathbf{z}}$	0.00482 $\hat{\mathbf{z}}$
TW_2	0.1776	0.1533	1.306	$\{e, \sigma_z\tau_x\}$	3	2	0.3959 $\hat{\mathbf{x}}$	0.0879 $\hat{\mathbf{x}}$
TW_3	0.2515	0.1520	1.534	$\{e, \sigma_z\tau_x\}$	4	2	0.4646 $\hat{\mathbf{x}}$	0.1532 $\hat{\mathbf{x}}$

TABLE 2. Properties of traveling-wave solutions for Ω_{W03} cell, $Re = 400$, defined as in table 1, with wave velocity $\mathbf{c}$ and mean velocity. See also figure 8 (a).

5. Bifurcations under *Re*

The relations between the equilibrium and traveling-wave solutions can be clarified by tracking their properties under changes in Re and cell size variations. Figure 10 shows a bifurcation diagram for equilibria and traveling waves in the Ω_{W03} cell, with dissipation rate D plotted against Re as the bifurcation parameter. A number of independent solution curves are shown in superposition. This is a 2-dimensional projection from the ∞-dimensional state space, thus, unless noted otherwise, the apparent intersections of the solution curves do not represent bifurcations; rather, each curve is a family of solutions with an upper and lower branch, beginning with a saddle-node bifurcation at a critical Reynolds number.

The first saddle-node bifurcation gives birth to the Nagata lower branch EQ_1 and upper

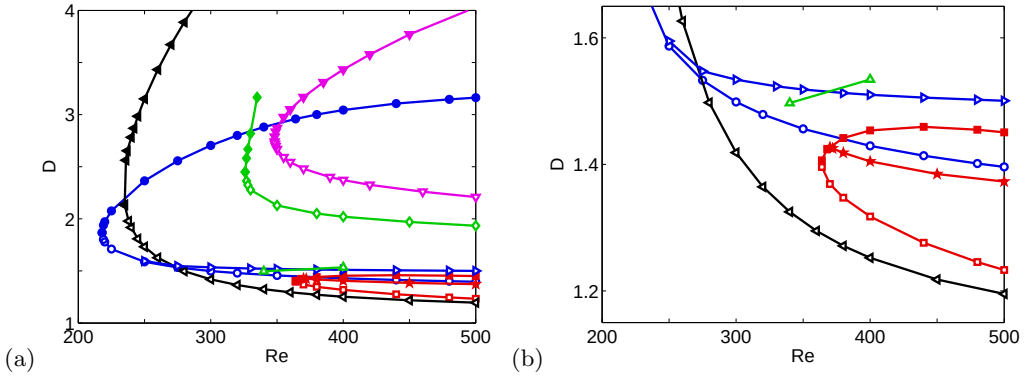

FIGURE 10. (a) Dissipation rate as a function of Reynolds number for all equilibria in in the Ω_{W03} cell. (b) Detail of (a). ○ EQ_1, ● EQ_2, □ EQ_3, ■ EQ_4, ◊ EQ_5, ♦ EQ_6, ◁ EQ_7, ◀ EQ_8, ★ EQ_9, ▽ EQ_{10}, ▼ EQ_{11}, ▷ TW_1, and △ TW_3.

branch EQ_2 equilibria, at $\text{Re} \approx 218.5$. EQ_1 has a single S-isotropic unstable eigenvalue (and additional subharmonic instabilities that break the S-isotropy of EQ_1). Shortly after bifurcation, EQ_2 has an unstable complex eigenvalue pair within the S-invariant subspace and two unstable real eigenvalues leading out of that space. As indicated by the gentle slopes of their bifurcation curves, the Nagata (1990) solutions are robust with respect to Reynolds number. The lower branch solution has been continued past $\text{Re} = 10,000$ and has a single unstable eigenvalue throughout this range (Wang *et al.* 2007).

EQ_3 and EQ_4 were discovered in independent Newton searches and subsequently found by continuation to be lower and upper branches of a saddle-node bifurcation occurring at $Re \approx 364$. EQ_3 has a leading unstable complex eigenvalue pair within the S-invariant subspace. Its remaining two unstable eigen-directions are nearly marginal and lead out of this space.

EQ_6 was found by continuing EQ_5 backwards in Re around the bifurcation point at $Re \approx 326$. We were not able to continue EQ_6 past $Re = 330$. At this point it has a nearly marginal stable pair of eigenvectors whose isotropy group is Γ, which rules out a bifurcation to traveling waves along these modes. Just beyond $Re = 330$ the dynamics in this region appears to be roughly periodic, suggesting that EQ_6 undergoes a supercritical Hopf bifurcation here. At $Re \approx 348$, EQ_{10} / EQ_{11} are born in a saddle node bifurcation, similar in character to the EQ_1 / EQ_2 bifurcation.

Figure 10(b) shows several symmetry-breaking bifurcations. At $Re \approx 250$, TW_1 bifurcates from EQ_1 in a subcritical pitchfork as an s_2-symmetric, s_1, s_3-antisymmetric eigenfunction of EQ_1 becomes unstable, resulting in a spanwise-moving traveling wave. At $Re \approx 370$, the EQ_9 equilibrium bifurcates off EQ_4 along an σ_{xz}-symmetric, s_1, s_2-antisymmetric eigenfunction of EQ_4. Since σ_{xz} symmetry fixes phase in both x and z, this solution bifurcates off EQ_4 as an equilibrium rather than a traveling wave.

6. Bifurcations under spanwise width L_z

In this section we examine changes in solutions under variation in spanwise periodicity. In particular, we are interested in connecting the solutions for Ω_{W03} discussed in § 4, to the wider Ω_{HKW} cell of Hamilton *et al.* (1995), which empirically exhibits turbulence for long time scales at $Re = 400$. Figure 11 shows dissipation as a function of L_z. Of the equilibria discussed above, only EQ_4, EQ_7, and EQ_9 could be continued from Ω_{W03} to Ω_{HKW} at $Re = 400$. The other equilibria terminate in saddle-node bifurcations, or

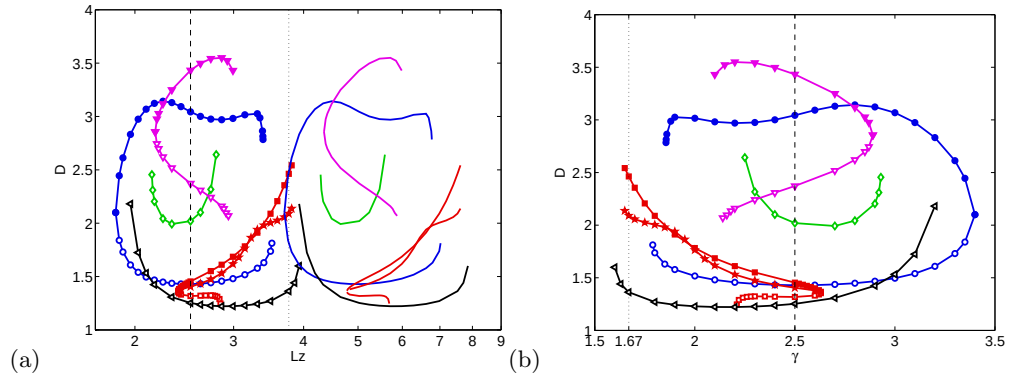

FIGURE 11. Dissipation rate D of equilibria for family of cells $\Omega(L_z) = [2\pi/1.14, 2, L_z]$ as function of (a) the spanwise cell width L_z (b) wavenumber $\gamma = 2\pi/L_z$. The vertical dashed lines represent the $\Omega_{\rm W03}$ cell at $L_z = 2.51$, $\gamma = 2.5$, and the vertical dotted line marks the $\Omega_{\rm HKW}$ cell at $L_z = 3.76$, $\gamma = 1.67$. ○ EQ_1, ● EQ_2, □ EQ_3, ■ EQ_4, ◊ EQ_5, ◁ EQ_7 ★ EQ_9, ▽ EQ_{10}, ▼ EQ_{11}. The repeated solution curves at doubled values of L_z indicate solutions of fundamental periodicity L_z embedded in a cells with spanwise length $2L_z$. (see figure 12). Equilibria ♦ EQ_6, ◀ EQ_8 do not exist at $Re = 400$. We did not attempt to continue TW_1, TW_2, or TW_3 in L_z.

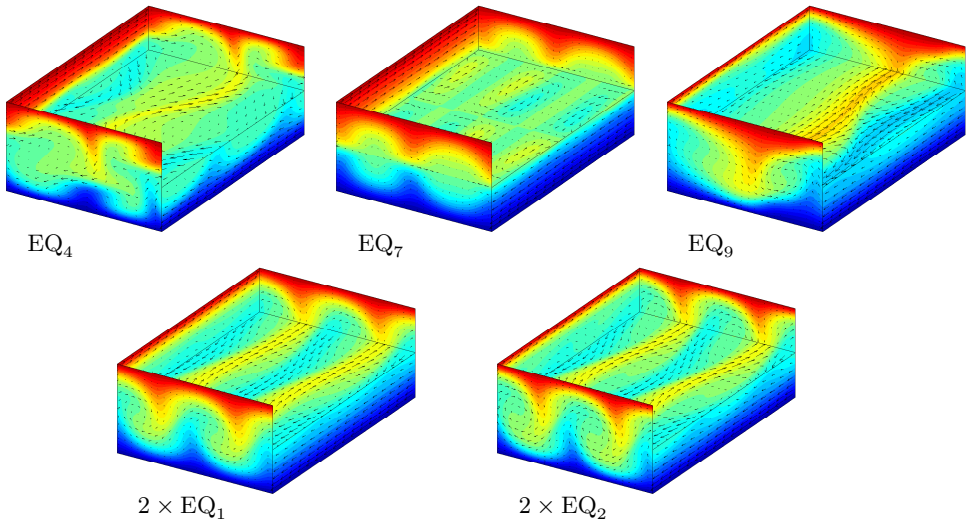

FIGURE 12. Equilibria in the $\Omega_{\rm HKW}$ cell of Hamilton *et al.* (1995), $Re = 400$. EQ_4, EQ_7, EQ_9, and the spanwise-doubled equilibrium solutions $2 \times \mathrm{EQ}_1$ and $2 \times \mathrm{EQ}_2$.

bifurcate into pairs of traveling waves in pitchfork bifurcations. EQ_1 and EQ_2 exist in $\Omega_{\rm HKW}$ as spanwise doubled $2\times\mathrm{EQ}_1$ and $2\times\mathrm{EQ}_2$ in z. We insert 2 copies of the EQ_1 / EQ_2 solution for $\Omega_{\rm W03}$, with $L_z \approx 2.51$, into a cell with $L_z \approx 5.02$, and then continue these solutions down to the $\Omega_{\rm HKW}$ width $L_z = 3.76$. Figure 12 shows 3D velocity fields for all of these equilibria in $\Omega_{\rm HKW}$: EQ_4, EQ_7, and EQ_9 and the spanwise doubled $2 \times \mathrm{EQ}_1$ and $2 \times \mathrm{EQ}_2$. Their properties are listed in table 6.

In the $\Omega_{\rm HKW}$ cell EQ_4 is extremely unstable, with a 39 dimensional unstable manifold. In physical space it has 4 distinct streaks, see figure 12. Owing to its near τ_z symmetry, many of its eigenvalues appear in sets of two nearly identical complex pairs.

The low dissipation values of the $\Omega_{\rm HKW}$ equilibria figure 8 (b) suggest that they are not involved in turbulent dynamics, except perhaps as gatekeepers to the laminar equilib-

	$\|\cdot\|$	E	D	H	$\dim W^u$	$\dim W^u_H$
mean	0.40	0.15	3.0			
EQ_0	0	0.1667	1	Γ	0	0
$2\times EQ_1$	0.2458	0.1112	1.8122	$S \times \{e, \tau_z\}$	5	0
$2\times EQ_2$	0.3202	0.0905	2.4842	$S \times \{e, \tau_z\}$	6	0
EQ_4	0.2853	0.0992	2.4625	S	40	13
EQ_7	0.1261	0.1433	1.3630	$S \times \{e, \tau_{xz}\}$	6	2
EQ_9	0.3159	0.1175	2.0900	$\{e, \sigma_{xz}\}$	11	0

TABLE 3. Properties of equilibrium and traveling wave solutions for Ω_{HKW} cell, $Re = 400$, defined as in table 1. See also figure 8 (b).

rium. We suspect that the equilibria as yet undiscovered, or the already known periodic orbit solutions (Gibson *et al.* 2008*a*) do play a key role in organizing turbulent dynamics. However, unlike the Ω_{W03} cell, we were not able to find any equilibria for Ω_{HKW} cell from initial guesses sampled from long-time turbulent trajectories within the S-invariant subspace. This is curious, contrasted to our success in finding equilibria from such guesses in Ω_{W03}, and suggests that the aspect ratios of the Ω_{HKW} cell are the most incommensurate (fit the intrinsic widths of rolls least well) compared to the roll and streak scales of spanwise-infinite domains, which are apparent (approximately) in the simulation of figure 2.

7. Conclusion and perspectives

As a turbulent flow evolves, every so often we catch a glimpse of a familiar pattern. For any finite spatial resolution, the flow approximately follows for a finite time a pattern belonging to a finite alphabet of admissible fluid states, represented here by a set of exact equilibrium and traveling wave solutions of Navier-Stokes. These are not the 'modes' of the fluid, in the sense that they would offer a lower-dimensional basis set to represent the flow with, and they are not a decomposition of the flow into a sum of different wavelength scale components; each solution spans the whole range of physical scales of the turbulent fluid, from the outer wall-to-wall scale, down to the Kolmogorov viscous dissipation scale. Numerical computations have to be carried out in a DNS representation of sufficient resolution to cover all of these scales, so no dimensional reduction is likely, beyond the improvement of numerical codes. The role of exact invariant solutions of Navier-Stokes is, instead, to partition the ∞-dimensional state space into a finite set of neighborhoods visited by a typical long-time turbulent fluid state.

Motivated by the recent observations of recurrent coherent states in experiments and numerical studies, we undertook here an exploration of the hierarchy of all known exact equilibria and traveling waves of fully-resolved plane Couette flow in order to describe the spatio-temporally chaotic dynamics of transitionally turbulent fluid flows. Turbulent plane Couette dynamics visualized in state space appears pieced together from close visitations to exact coherent states connected by transient interludes, as can be seen in Gibson (2008*b*) animations of figure 2. The $3D$ fluid states explored by the small cell aspect ratio equilibria and their unstable manifolds studied in this paper are strikingly similar to states observed in larger aspect cells, such as figure 2.

For plane Couette flow equilibria, traveling waves and periodic solutions embody a vision of turbulence as a repertoire of recurrent spatio-temporal patterns explored by turbulent dynamics. The new equilibria and traveling waves that we present here form

the backbone of this repertoire. Currently, a taxonomy of these myriad states eludes us, but emboldened by successes in applying periodic orbit theory to the simpler, warm-up Kuramoto-Sivashinsky problem (Christiansen *et al.* 1997; Lan & Cvitanović 2008; Cvitanović *et al.* 2008), we are optimistic. Given a set of equilibria, the next step is to understand how the dynamics interconnects the neighborhoods of the invariant solutions discovered so far; a task that we address in Halcrow *et al.* (2008) which discusses their heteroclinic inter-connections, and Gibson *et al.* (2008*a*) which discusses their periodic orbit solutions.

The reader might rightfully wonder what the small-aspect periodic cells studied here have to do with physical plane Couette flow and wall-bounded shear flows in general, with large aspect ratios and physical spanwise-streamwise boundary conditions. Indeed, the outstanding issue that must be addressed in future work is the small-aspect cell periodicities imposed for computational efficiency. So far, most computations of invariant solutions have focused on spanwise-streamwise (axial-streamwise in case of the pipe flow) periodic cells barely large enough to allow for sustained turbulence. Such small cells introduce dynamical artifacts such as lack of structural stability and cell-size dependence of the sustained turbulence states. However, every solution that we find is also a solution of the infinite aspect-ratio problem, i.e., a solution whose finite $[L_x, 2, L_z]$ cell tiles the infinite $3D$ plane Couette flow. As we saw in § 6, under a continuous variation of spanwise length L_z such solutions come in continuous families whose fundamental wavelengths reflect the roll and streak instability scales observed in large-aspect systems such as figure 2. Here we can draw the inspiration from pattern-formation theory, where the most unstable wavelengths from a continuum of unstable solutions set the scales observed in simulations.

We would like to acknowledge F. Waleffe for providing his equilibrium solution data and for his very generous guidance through the course of this research. We greatly appreciate discussions with D. Viswanath, his guidance in numerical algorithms, and for providing his traveling wave data. We are indebted to G. Kawahara, L.S. Tuckerman, B. Eckhardt, D. Barkley, and J. Elton for inspiring discussions. P.C., J.F.G. and J.H. thank G. Robinson, Jr. for support. J.F.G. was partly supported by NSF grant DMS-0807574. J.H. thanks R. Mainieri and T. Brown, Institute for Physical Sciences, for partial support. Special thanks to the Georgia Tech Student Union which generously funded our access to the Georgia Tech Public Access Cluster Environment (GT-PACE), essential to the computationally demanding Navier-Stokes calculations.

REFERENCES

Canuto, C., Hussaini, M. Y., Quarteroni, A. & Zang, T. A. 1988 *Spectral Methods in Fluid Dynamics*. Springer-Verlag.

Christiansen, F., Cvitanović, P. & Putkaradze, V. 1997 Spatio-temporal chaos in terms of unstable recurrent patterns. *Nonlinearity* **10**, 55–70.

Clever, R. M. & Busse, F. H. 1997 Tertiary and quaternary solutions for plane Couette flow. *J. Fluid Mech.* **344**, 137–153.

Cvitanović, P., Davidchack, R. L. & Siminos, E. 2008 State space geometry of a spatio-temporally chaotic Kuramoto-Sivashinsky flow. `arXiv:0709.2944`, submitted to SIAM J. Applied Dynam. Systems.

Frisch, U. 1996 *Turbulence*. Cambridge, UK: Cambridge University Press.

Gibson, J. F. 2008*a* Channelflow: a spectral Navier-Stokes simulator in C++. *Tech. Rep.*. Georgia Inst. of Technology, `Channelflow.org`.

Gibson, J. F. 2008*b* Movies of plane Couette. *Tech. Rep.*. Georgia Institute of Technology, `ChaosBook.org/tutorials`.

Gibson, J. F., Halcrow, J. & Cvitanović, P. 2008*a* A survey of relative periodic solutions of moderate *Re* plane Couette flow. In preparation.

Gibson, J. F., Halcrow, J. & Cvitanović, P. 2008*b* Visualizing the geometry of state-space in plane Couette flow. *J. Fluid Mech.* **611**, 107–130, `arXiv:0705.3957`.

Gilmore, R. & Letellier, C. 2007 *The Symmetry of Chaos*. Oxford: Oxford Univ. Press.

Golubitsky, M. & Stewart, I. 2002 *The symmetry perspective*. Boston: Birkhäuser.

Halcrow, J. 2008 Geometry of turbulence: An exploration of the state-space of plane Couette flow. PhD thesis, School of Physics, Georgia Inst. of Technology, Atlanta, `ChaosBook.org/projects/theses.html`.

Halcrow, J., Gibson, J. F., Cvitanović, P. & Viswanath, D. 2008 Heteroclinic connections in plane Couette flow. `arXiv:0808.1865`, submitted to J. Fluid Mech.

Hamilton, J. M., Kim, J. & Waleffe, F. 1995 Regeneration mechanisms of near-wall turbulence structures. *J. Fluid Mech.* **287**, 317–348.

Harter, W. G. 1993 *Principles of Symmetry, Dynamics, and Spectroscopy*. New York: Wiley.

Hoyle, R. 2006 *Pattern Formation: An Introduction to Methods*. Cambridge: Cambridge Univ. Press.

J.E. Dennis, Jr., & Schnabel, R. B. 1996 *Numerical Methods for Unconstrained Optimization and Nonlinear Equations*. Philadelphia: SIAM.

Jiménez, J., Kawahara, G., Simens, M. P., Nagata, M. & Shiba, M. 2005 Characterization of near-wall turbulence in terms of equilibrium and bursting solutions. *Phys. Fluids* **17**, 015105.

Kim, H., Kline, S. & Reynolds, W. 1971 The production of turbulence near a smooth wall in a turbulent boundary layer. *J. Fluid Mech.* **50**, 133–160.

Kleiser, L. & Schuman, U. 1980 Treatment of incompressibility and boundary conditions in 3-D numerical spectral simulations of plane channel flows. In *Proc. 3rd GAMM Conf. Numerical Methods in Fluid Mechanics* (ed. E. Hirschel), pp. 165–173. GAMM, Viewweg, Braunschweig.

Lan, Y. & Cvitanović, P. 2008 Unstable recurrent patterns in Kuramoto-Sivashinsky dynamics. *Phys. Rev. E* **78**, 026208, `arXiv.org:0804.2474`.

Marsden, J. E. & Ratiu, T. S. 1999 *Introduction to Mechanics and Symmetry*. New York, NY: Springer-Verlag.

Nagata, M. 1990 Three-dimensional finite-amplitude solutions in plane Couette flow: bifurcation from infinity. *J. Fluid Mech.* **217**, 519–527.

Nagata, M. 1997 Three-dimensional traveling-wave solutions in plane Couette flow. *Phys. Rev. E* **55** (2), 2023–2025.

Peyret, R. 2002 *Spectral Methods for Incompressible Flows*. Springer-Verlag.

Schmiegel, A. 1999 Transition to turbulence in linearly stable shear flows. PhD thesis, Philipps-Universität Marburg, available on `archiv.ub.uni-marburg.de/diss/z2000/0062`.

Schneider, T., Gibson, J., Lagha, M., Lillo, F. D. & Eckhardt, B. 2008 Laminar-turbulent boundary in plane Couette flow. *Phys. Rev. E.* **78**, 037301, `arXiv:0805.1015`.

Skufca, J. D., Yorke, J. A. & Eckhardt, B. 2006 Edge of chaos in a parallel shear flow. *Phys. Rev. Lett.* **96** (17), 174101.

Tuckerman, L. S. & Barkley, D. 2002 Symmetry breaking and turbulence in perturbed plane Couette flow. *Theoretical and Computational Fluid Dynamics* **16**, 91–97, `arXiv:physics/0312051`.

Viswanath, D. 2007 Recurrent motions within plane Couette turbulence. *J. Fluid Mech.* **580**, 339–358, `arXiv:physics/0604062`.

Viswanath, D. 2008 The dynamics of transition to turbulence in plane Couette flow. In *Mathematics and Computation, a Contemporary View. The Abel Symposium 2006*, *Abel Symposia*, vol. 3. Berlin: Springer-Verlag, `arXiv:physics/0701337`.

Waleffe, F. 1990 Proposal for a self-sustaining mechanism in shear flows. Center for Turbulence Research, Stanford University/NASA Ames, unpublished preprint (1990).

Waleffe, F. 1995 Hydrodynamic stability and turbulence: beyond transients to a self-sustaining process. *Stud. Applied Math.* **95**, 319–343.

Waleffe, F. 1997 On a self-sustaining process in shear flows. *Phys. Fluids* **9**, 883–900.

Waleffe, F. 1998 Three-dimensional coherent states in plane shear flows. *Phys. Rev. Lett.* **81**, 4140–4143.

Waleffe, F. 2003 Homotopy of exact coherent structures in plane shear flows. *Phys. Fluids* **15**, 1517–1543.

Wang, J., Gibson, J. F. & Waleffe, F. 2007 Lower branch coherent states in shear flows: transition and control. *Phys. Rev. Lett.* **98** (20).